# On the use of meteorological observations in SAR interferometry*

Ramon Hanssen[1,2], Howard Zebker[2], Roland Klees[1], and Sylvia Barlag[3]
[1]DEOS, Delft University of Technology, Thijsseweg 11, 2629 JA Delft, the Netherlands
Phone: +31 15 2782562 (fax: 3711) email: hanssen@geo.tudelft.nl, klees@geo.tudelft.nl
[2]STAR Laboratory, Stanford University, Stanford CA, 94305-9515 USA
Phone: +1 650 723 8067 (fax: 57344) email: zebker@jakey.stanford.edu
[3]Royal Netherlands Meteorological Institute (KNMI),
PO Box 201, 3730 AE, De Bilt, The Netherlands, email: barlag@knmi.nl

*Abstract* **We studied a series of 26 SAR interferograms to examine the variation in the interferometric phase, caused by spatial variability in atmospheric propagation delay. Meteorological observations confirm the driving mechanisms behind this variability. We comment on the potential of meteorological data to assess the interferogram quality a priori. Weather radar and synoptic observations give a good indication for strong atmospheric signal, while weather satellite images can be used for reconnaissance if acquired within an hour from the SAR acquisitions.**

## INTRODUCTION

The feasibility of repeat-pass SAR interferometry for monitoring deformation processes and measuring elevation is often limited by atmospheric heterogeneity at the acquisition times. Although localized interferometric phase shifts due to atmospheric delay can sometimes be identified using reference elevation models, the combination with, e.g., temporal decorrelation in particular hampers data interpretation considerably.

Both a deterministic and a statistical approach can be followed to address the problem of atmospheric artifacts in SAR interferograms. Stacking and averaging multiple interferograms of the same area can be used to suppress atmospheric signal for topographic applications. For deformation studies, however, strong assumptions would need to be made about deformation rates, which significantly reduce the potential of the interferometric observations. Furthermore, power law relationships [1], needed for some statistical approaches and often applied in other areas of signal propagation modeling, appear to be of limited use, e.g., for localized convective processes.

We investigate the potential of meteorological data to assess the quality of an interferogram a priori. As a first exercise, we attempt to explain the observed interferometric anomalies in a series of 26 interferograms of the Netherlands, using a wide range of simultaneous meteorological observations [2]. We find proof for the influence of water vapor distribution, clouds, rain and temperature gradients. This experience is then used to comment on the use of different types of meteorological observations for SAR interferometry, which can be valuable information for the selection of suitable SAR pairs, or for weighting SAR scenes in a stack of interferograms.

It is well known that spatial differences in the ionosphere can cause differences in the propagation speed of the signal. However, since the ionospheric spatial variability is not well known at these relatively small scales, and the interferometric observations have an inherently relative character, we focus on tropospheric influence in this study. In fact, all observed anomalies could be explained by tropospheric parameters.

## ATMOSPHERIC SIGNAL

Atmospheric signal in SAR interferograms is due to the spatial variability of the refractive index of the propagation medium. The sensitivity for atmospheric signal is confined to a spatial range from approximately 50–100 meters to 50–100 km, dictated by resolution cell size and standard image size respectively. In this range, especially the water vapor, rain, and clouds influence the variability. Pressure and temperature have a much smoother spatial behavior, causing long wavelength phase variations which can be difficultly discerned from orbit errors.

The coherent spatial variation of the interferometric phase, $d\varphi$, in a repeat-pass interferogram, neglecting any possible deformations or penetration differences, can be described by:

$$d\varphi = \frac{4\pi}{\lambda}\left(\frac{B^{\perp}}{R_1 \sin\theta} dH + d\Delta R_{e,1} - d\Delta R_{e,2}\right), \quad (1)$$

where $\lambda$ is the radar wavelength, $B^{\perp}$ is the perpendicular baseline, $R_1$ is the slant range to the reference satellite

*Presented at the International Geoscience and Remote Sensing Symposium, 6-10 July 1998, Seattle, WA

pass, $\theta$ is the look angle, $H$ is the topographic height, and $\Delta R_{e,i}$ is the propagation delay to satellite pass $i$. The first term in the brackets shows the topographic component, which scales with the perpendicular baseline, whereas the two delay components are baseline independent. The across track and along track derivatives of the propagation delays and the topographic height cause the variation of the interferometric phase. Here we assume that the topography is known, and the propagation delays constitute the dominant interferometric signal.

Though in other fields of space geodetic measurements the absolute propagation delay $\Delta R_e$ needs to be determined, in SAR interferometry only spatial variations in propagation delay $d\Delta R_e$ can be observed. We distinguish between clear air and liquid induced delay. Clear air delay is routinely described by the hydrostatic delay and the wet delay, which is caused by the permanent dipole moment of water vapor refractivity [3].

The hydrostatic delay can be written as:

$$\Delta R_{e,\mathrm{HD}} = 10^{-6} \frac{k_1 R_d}{g_m \cos\theta} P_s, \qquad (2)$$

with $k_1$ a constant [4], $R_d$ the specific gas constant for dry air, $g_m$ the approximate local gravity at the centroid of the atmospheric column [5], and $P_s$ the surface pressure. For the test sites in this study, $d\Delta R_{e,\mathrm{HD}} = 2.3 \cdot 10^{-3} dP_s$, approximately 2 mm delay per hPa surface pressure change. Since pressure gradients are usually limited (less than 0.05–0.1 hPa/km) within an area of 100 × 100 km, this will result in long wavelength phase variation, which is mostly eliminated while flattening the interferogram.

Much shorter wavelengths can be expected from the wet delay; the combination of water vapor and temperature:

$$\Delta R_{e,\mathrm{WD}} = \frac{10^{-6}}{\cos\theta} \int_0^H (k_2' \frac{e}{T} + k_3 \frac{e}{T^2}) dh, \qquad (3)$$

where $k_2'$ and $k_3$ are constants [4], $e$ is the partial pressure of water vapor, and $T$ is the temperature. The vertical integration spans the total height of the tropospheric column. Maximum spatial variations observed in this study reach up to 4.5 cm in one SAR image. An interferometric combination with two strongly variable situations reaches up to 9 cm variation. This variation occurred over a spatial range of about 10 km.

Apart from the clear air effect, liquid particles such as cloud droplets induce an additional dispersive delay. This delay is related to the liquid water content $W$ in g/m$^3$ [6], and its dominating non-dispersive part can be written as:

$$\Delta R_{e,\mathrm{cloud}} \quad [\text{in mm}] = \frac{1.45}{\cos\theta} W \quad [\text{per km}]. \qquad (4)$$

For cumulus and cumulonimbus clouds, this delay reaches values of 0.7–3 mm/km, adding up to the cm-level for vertically developed cumulonimbus clouds. Since strong cumulonimbus clouds have diameters around 10 km, these effects are significant in the interferometric observations.

## METEOROLOGICAL OBSERVATIONS

We study synoptic observations, weather radar, radiosondes, spaceborne images, and weather charts for comparison with the interferograms.

Synoptic observations are simultaneously obtained by a large number of manned or unmanned stations. Automatic observations mostly include temperature, pressure, relative humidity, amount of precipitation, wind speed and direction, and solar radiation. Manually, the weather is coded in a weather category, the horizontal visibility is estimated, and cloud cover, type, and height is observed. All observations are coded into standardized tables.

The weather radar measures the intensity of microwave scattering from precipitation particles, and uses azimuth and elevation ranging for geolocating the return signal and estimating the maximum height of the reflections. The scatter intensity is converted in precipitation rate in mm/hr. Using a beam with of 1 degree, the resolution decreases with increasing range. The observations are nearly continuous.

Radiosonde data are acquired worldwide at the synoptic hours, and provide vertical profiles of temperature, pressure, relative humidity and wind direction and velocity. These data are usually plotted in a thermodynamic diagram, which gives a convenient insight in, e.g., the stability of the atmosphere, cloud levels, and inversion layers.

Meteorological satellites use different wavelength bands, providing information on, e.g., integrated water vapor, infrared radiation and radiation in the visible part of the spectrum. We use NOAA-AVHRR, with a temporal sampling of approximately 6 hours, and a spatial resolution of 1.1 × 1.1 km at nadir, and Meteosat, with a temporal sampling of 30 minutes and a spatial resolution of 5 × 5 km at nadir.

Standard weather charts are provided by national and international meteorological services, and are usually based on synoptic scale meteorological models. The data assimilation part of these models currently samples at a spatial scale of 50 km or more. Therefore, these charts mainly show the location of highs and lows and frontal systems. In the charts, often surface observations are plotted, giving information on temperature, wind, total cloud cover, and precipitation.

## INTERFEROGRAM ANALYSIS

Analysis of the 26 interferograms shows that weather radar observations of precipitation have in most cases a high correlation with observed anomalies in the interferograms. As an example, Fig.1 shows a differential interferogram over the southwest of the Netherlands, with

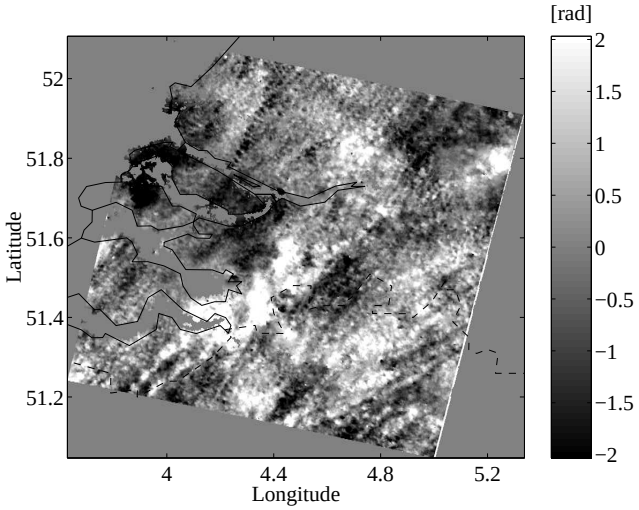


Figure 1: Phase of the geocoded differential interferogram over Delft, the Netherlands, April 23 and 24, 1996, 10:38 UTC.

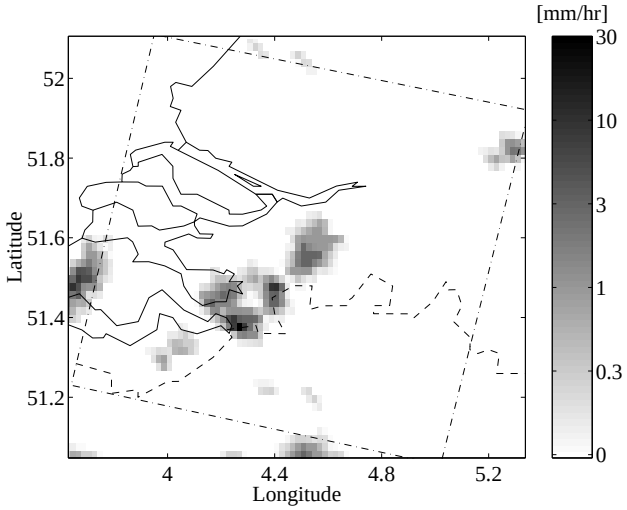


Figure 2: Weather radar over Delft, the Netherlands, April 24, 1996, 10:30 UTC. Precipitation rate in mm/hr.

some isolated anomalies. The weather radar precipitation image of the second acquisition in Fig.2 shows rain cells at the same position as the interferogram anomalies. The weather radar image corresponding to the first SAR acquisition (not shown here) shows precipitation at the positions of the negative anomalies in the interferogram. Since convective processes cause an increase in the horizontal water vapor variability, the phase disturbances are mainly caused by water vapor differences, in combination with the effects of rain and clouds. Laminar and turbulent transport of water vapor is observed in many of the interferograms.

In all situations in which the synoptic cloud observations indicated cumulus or cumulonimbus clouds, the interferograms showed localized phase anomalies, in the form of cells or more elongated features. Stratus or cirrus cloud observations did not show this strong effect, although often small ripples occur in the interferogram, probably caused by inhomogeneities in the cloud cover. Other important synoptic information is the amount of rain fall, which does not require manual observation, and is therefore available at more synoptic stations.

Comparing summer and winter interferograms, it is found that the highest rms values are found in summer observations. This is due to temperature differences, causing more convectivity. Useful interferograms are expected during stable weather conditions, i.e., preferably night time (ascending) acquisitions and winter acquisitions.

Gravity waves are observed in 8 of the 26 interferograms. The radiosonde profiles indicated inversions or saturated layers in all of these cases, which could cause gravity waves in combination with, e.g., wind shear. Due to the often relatively long time differences between the SAR acquisitions and the radiosonde launches (1.5–3.5 hours), combined with the sparse spatial sampling, these data are of limited use.

Temporally coinciding weather satellite observations prove to be useful for the detection of storm fronts, or regions of strong atmospheric instability. However, they can hardly be used for the identification of single anomalies with a diameter smaller than approximately 10 km. For two interferograms, the Meteosat water vapor image identified strong water vapor trends which were not visible in other meteorological observations.

## CONCLUSIONS

Indications for atmospheric signal in SAR interferograms are convective clouds, rain, water vapor variability, and fronts. Smaller signal originates from gravity waves. Weather radar is of great value identifying precipitation, but is unfortunately not everywhere available. Synoptic observations of cloud types and precipitation is both valuable and available over most areas. Conveniently archived are weather satellite images, where high resolution images acquired closest to the SAR acquisitions are preferred. For time lags of more than approximately 1 hour, it becomes difficult to correlate the observed structures with the SAR images. Radiosonde data and weather charts are of less value due their poor spatial sampling.

## ACKNOWLEDGMENT

The authors would like to thank the European Space Agency for support and providing the ERS SAR data.

## REFERENCES


[1] R. Goldstein. "Atmospheric limitations to repeat-track radar interferometry," Geophysical Research Letters, vol. 22, pp. 2517–2520, Sept. 1995.

[2] R. Hanssen, "Assessment of the role of atmospheric heterogeneities in ERS tandem SAR interferometry," Report for the European Space Agency, in press, 1998.

[3] J.L. Davis, T.A. Herring, I.I. Shapiro, A.E.E. Rogers, and G. Elgered. "Geodesy by radio interferometry: Effects of atmospheric modeling errors on estimates of baseline length," Radio Science, vol. 20, pp. 1593–1607, 1985.

[4] E.K. Smith, Jr. and S. Weintraub "The constants in the equation for atmospheric refractive index at radio frequencies," Proceedings of the I.R.E, vol. 41, pp. 1035–1037, Aug. 1953.

[5] J. Saastamoinen. "Introduction to practical computation of astronomical refraction," Bulletin Geodesique, vol. 106, pp. 383–397, 1972.

[6] F.S. Solheim, J. Vivekanandan, R.H. Ware, and C. Rocken, "Propagation delays induced in GPS signals by dry air, water vapor, hydrometeors and other particulates," unpublished, 1997.